Computational Structural, Electronic and Optical Properties of the Palmitic Acid in its C Form

J. G. S. Santos
Universidade Estadual do Piaui
A. MACEDO-FILHO (amfilho@prp.uespi.br)
Universidade Estadual do Piauí https://orcid.org/0000-0002-9419-5595
A. M. Silva
Universidade Estadual do Piaui
F. F. de Sousa
Universidade Federal do Para
E. W. S. Caetano
Instituto Federal de Educacao, Ciencia e Tecnologia do Ceará
M. B. da Silva
Universidade Federal do Ceara
V. N. Freire
Universidade Federal do Ceara

Research Article

Keywords: DFT calculations, Palmitic acid, Semiconducting behavior

Posted Date: March 17th, 2021

DOI: https://doi.org/10.21203/rs.3.rs-299903/v1

Journal of Molecular Modeling manuscript No.
(will be inserted by the editor)

Computational Structural, Electronic and Optical Properties of the Palmitic Acid in its C Form

J. G. S. Santos · A. Macedo-Filho · A. M. Silva · F. F. de Sousa · E. W. S. Caetano · M. B. da Silva · V. N. Freire

Received: date / Accepted: date

Abstract In this work, we report a theoretical study of the structural, electronic, and optical properties of palmitic acid crystal in its C form under DFT calculations level. Palmitic acid is a fatty acid that constitutes the large majority of vegetable oils with recognized potential applications in medicine, pharmaceuticals, cosmetics technology, foods, and fuel. As a main result, we have found that the electronic bandstructure reveals indirect gap $3.713eV$ ($E \longrightarrow B$ and $E \longrightarrow \Gamma$), as a main bandgap, while the secondary bandgaps found were $4.175eV$ ($\gamma_1 \longrightarrow \Gamma$) and $4.172eV$ ($\gamma_2 \longrightarrow B$). It behaves like a wide bandgap semiconductor, which points to potential applications in optoelectronic devices.

Keywords DFT calculations · Palmitic acid · Semiconducting behavior

J. G. S. Santos, A. Macedo-Filho
PPGQ-GERATEC, Universidade Estadual do Piauí, 64002-150, Teresina-PI, Brazil

A. Macedo-Filho
Departamento de Física, Universidade Estadual do Piauí, 64002-150 Teresina-PI, Brazil E-mail: amfilho@prp.uespi.br

A. M. Silva
Campus Prof. Antonio Geovanne Alves de Sousa, Universidade Estadual do Piauí, 64260-000 Piripiri-PI, Brazil

F. F. de Sousa
Faculdade de Física, Universidade Federal do Pará, 66075-110, Belém, PA, Brazil

E. W. S. Caetano
Instituto Federal de Educação, Ciência e Tecnologia do Ceará, DEMEL, Campus Fortaleza, 60040-531 Fortaleza-CE, Brazil

M. B. da Silva, V. N. Freire
Departamento de Física, Universidade Federal do Ceará, 60455-760 Fortaleza-CE, Brazil

1 Introduction

Currently, fatty acids have attracted the attention of the scientific community. Due to their fundamental properties, it has potential application in the medicine, pharmaceuticals, cosmetics technology, foods, and fuel fields [1–8], which requires great efforts to synthesize and characterize fatty acid crystals through experimental techniques. In this context, from an experimental or theoretical point of view, there is a fundamental importance to obtain better potentialities and overall properties comprehension of such structure [9–15].

Fatty acids are organic compounds constituted of an oxygenated function so-called carboxylic acid, following the general molecular formula $CH_3(CH_2)_xCOOH$. Here, x is the number of carbon atoms in the hydrocarbon chain. The hydrocarbons chains vary from 4 to 36 carbons, differing only by the number of carbon atoms in their chains [16]. On the other hand, although the chains have similar crystalline structures, they display complex polymorphism [17, 18], something frequently observed in organic molecules [19].

Varieties of polymorphic forms are related to the structure of the chain, which depend on the carbon number, the chain size and the parity [20]. With regard to parity, the A_1, A_2, A_3, A_{super}, C, $B_{o/m}$ and $E_{o/m}$ forms are observed in even fatty acids, while the A', B', C', C'' and D' forms are observed in odd fatty acids [18, 21–25]. In addition, in some cases, the fatty acids chains are saturated. For instance, the lauric (12:0,C_{12}), myristic (14:0, C_{14}), palmitic (16:0, C_{16}), estearic (18:0, C_{18}), arachidic (20:0, C_{20}) and arachidonic (20:4, C_{20}) acids. On the other hand, as unsaturated chains we cite the palmitoleic (16:1, C_{16}), oleic (18:1, C_{18}), linoleic (18:2, C_{18}), α-linolenic (18:3, C_{18}) and arachidonic (20:4, C_{20}) acids [16, 26]. Lastly, we still mentioning that there are fatty acids with short carbon chains with less than ten atoms in their chains, but are found in a minority in nature.

Regarding the polymorphism of fatty acids, it has drawn attention. It is synthesized in mammals, abundant in the blood flow, and also obtained from the diet. It is worth mentioning the treatment of skeletal muscle with palmitic acid for a long time involves insulin resistance development. On the other hand, acute exposure to this fatty acid can induce an increase in glucose uptake and oxidation, also an increase in glycogenic synthesis [27–29]. In this respect, this structure attaches a great deal with interest. Despite these facts, in this work, our main aim consists of a theoretical investigation of the palmitic acid, taking into account the palmitic acid crystal in its polymorphic C form under the density functional theory (DFT) technique. Here, we aim to obtain structural, electronic, and optical properties motivated by the nanotechnology advances in nanoelectronic devices.

Finally, this paper is organized as follows: in section 2 we describe the implementation of the DFT approach used. In section 3 we present our results and discussions about our proposed investigation. And finally, in section 4 we present our conclusions.

2 Computational approach

The unit cell of the palmitic acid crystal in its polymorphic C form, whose chemical formula is $CH_3(CH_2)_{14}COOH$, and its isolated molecule are both shown in Figs. 1(a) and 1(b), respectively. In addition, this crystal has a monoclinic symmetry belonging to the space group $P2_1/c$, and punctual group C_{2h}^5, with lattice parameters $a = 35.260(11)\mathring{A}$, $b = 4.9487(16)\mathring{A}$, $c = 9.406(3)\mathring{A}$, and volume $V = 1658.0\mathring{A}^3$. Its unit cell contains 4 molecules and $Z = 4$ organized periodically through dimers arranged as alternating monolayers of the carboxyl group and methyl radicals parallel to the plane (010), build-up by the hydrophilic part the carboxylic acid through hydrogen bonds [17]. Besides, we report that the configuration of the valence electrons for theoretical calculations are $2s^2 2p^2$ and $2s^2 2p^4$ for the carbon and hydrogen atoms, respectively.

Here, we investigate the monoclinic palmitic acid crystal in its C form. We implement computational approaches through the DFT method [30,31], employing the CASTEP code with Broyden-Fletcher-Goldfarb-Shanno (BFGS) algorithm [32–34], and the Local Density Approximation (LDA) approach [35,36] as the exchange-correlation functional both to optimize the unit cell geometry for the crystal under consideration. To address the crystal optimization, we used the LDA approximation with the cutoff energy value of 830eV [37,38].

3 Results and discussions

3.1 Structural properties

Table 1 shows the a, b and c unit cell lattice parameters, besides the V volume and β unit cell angle to palmitic acid in its C form. The experimental results [17] are also included for comparison purposes. Here, LDA calculations provided absolute deviations as follow, $\Delta a = 10.1\%$, $\Delta b = 35.2\%$, $\Delta c = 21.6\%$, $\Delta V = 56.0\%$ and $\Delta\beta = 16.5\%$ both in comparison to experimental data. We found theoretical results less than experimental measures, which occurs due to LDA calculations overestimate the bond forces among the atoms, obtaining smaller bond length and cell volume comparing to experimental measures.

Next, Table 2 shows the theoretical results (subscript L) for the length bond values among the oxygen, hydrogen, and oxygen atoms ($O\cdots H\cdots O$) in comparison to experimental measures (subscript E) [17]. Theoretical calculations depict that the bond amidst the hydrogen and the receptor oxygen atom ($H1\cdots O2$) shortened 33%. The length bond between oxygen atoms ($D\cdots A_L$) undergo a deviation around 8.9% in comparison to ($D\cdots A_E$). Here, we observe theoretical results greater than the experimental one with the emphasis on hydrogen bond of the donor atom ($D\cdots H_L$) around 24%. Regarding the hydrogen bonds angle deviations, we observe values close to $180\,^\circ$, which characterizes linear arrangement of molecules and stretching ν ($O\cdots H$) in the unit cell. The angular deviation between the theoretical and experimental results is about 0.8%.

3.2 Electronic properties

At first, Fig. 2 displays the first Brillouin zone and the unit cell of the palmitic acid in its C form depicting their, respective, high-symmetry points of its monoclinic structure given by Γ(0,0,0), Z(0,0,1/2), Y(0,1/2,0), A(-1/2,1/2,0), B(-1/2,0,0), C(0,1/2,1/2), D(-1/2,0,1/2), and E(-1/1,1/2,1/2). Kohn-Sham electronic band structure gives a glimpse of the electronic eigenenergies as a function of a set of quantum numbers that form the components of a wave vector in the first Brillouin zone of the analyzed crystal.

Fig. 3, shows the optimized electronic band structures of the crystal with their respective density of states. Close to the main bandgap are displayed the most relevant electronic transitions between the top of the valence band and the bottom of the conduction band. Following, on the right side, the s and p orbitals contribution through the electronic density of states (DOS) is depicted from -27.7 to $8.9eV$ range energy. The maximum valence band is located at the E high-symmetry point while the minimum conduction band is located at the Γ and B points, which characterizes an indirect transition with bandgap around $3.713eV$ ($E \longrightarrow B$ and $E \longrightarrow \Gamma$), besides to

Table 1 Lattice parameter (Å), unit cell volume (Å^3), and β angle ($^\circ$) obtained from the palmitic acid crystal in its C form using DFT calculations at the LDA level in comparison to experimental results. The deviations concerning experimental values are showed.

C. Level	a	Δa	b	Δb	c	Δc	V	ΔV	β	$\Delta\beta$
LDA_{830}	32.037	−3.583	3.201	−1.740	7.373	−2.033	729.228	−928.7724	105.389	14.942
Exp.	35.620	–	4.948	–	9.406	–	1657.970	–	90.447	–

Table 2 Theoretical calculations for the length bond values among the oxygen, hydrogen, and oxygen atoms (O · · · H · · · O) obtained from the palmitic acid crystal in its C form using DFT calculations at the LDA level. The measures concerning experimental values are showed.

$D-H\cdots A$	$D-H_L$	$D-H_E$	$H\cdots A_L$	$H\cdots A_E$	$D\cdots A_L$	$D\cdots A_L$	$O1-H1\cdots O_L$	$O1-H1\cdots O_E$
$O1-H1\cdots O2$	1.391	1.120	1.000	1.506	2.386	2.621	171.800	173.200

be the main bandgap. Next, secondary indirect transitions are observed, whose gap values are around $4.175eV$ and $4.172eV$ along the ($\gamma_1 \longrightarrow \Gamma$) and ($\gamma_2 \longrightarrow B$) paths, respectively. Here, the valence band located from -27.7 to $0eV$ range has its highest energy peak adjusted to $0eV$. The p orbitals of the atoms highlights at the top of the valence band besides the lowest energy levels of the conduction bands. For the lowest energies of the valence band, there is a prevalence of s orbitals, for presents less energy than p orbitals. At the top of the conduction band, we observe that both orbitals have very close densities, with the prominence of the s orbital.

Fig. 4, shows the partial density of states (PDOS) for the C (carbon), O (oxygen) and H (hydrogen) atoms, and CO, $COOH$ and OH functional groups. The C atom contributes from -18 to $0eV$ and 4.5 to $9eV$ ranges, with highlights to the p orbital. Following, O atom contributes from -27 to $-21eV$, with the s orbital, from -18 to $-1.5eV$ with the major contribution to the p orbital, and from 5.5 to $8eV$ with s and p orbitals contributing equivalently. Lastly, the H atom presents two pronounced peaks, being the major contribution in the range from -18 to $0eV$. Here, we can not see p orbital's contributions. Worth mentioning that each atom contributes to both valence and conduction bands.

Next, the carboxylic functional group highlights in the following ranges: 1) from -27.6 to $-21.6eV$, with major contribution of the s orbital; and 2) from -18.3 to $-1.6eV$ and from 5 to $9eV$ with predominance of the p orbital in both ranges. Like the carboxylic acid, the carbonyl function belongs to the same range, with the same set of orbitals contributing in each range. Similarly, the hydroxyl function belongs to the same range as the carboxylic and carbonyl functions. In the range from -27.6 to $-21.6eV$ the relevant contribution is the s orbital, while in the range from -18.3 to $-1.6eV$ the prominent contribution is the p orbital. Already in the conduction band, the major contribution is the p orbital for all functional groups.

Fig. 5, shows the effective mass calculated of the holes and electrons through the fitting quadratic curves (red dots) at points of interest around the Brillouin zone. Here, we aim to estimate the electronic transport behavior along the directions of the crystal from the maximum point of the valence band (holes) and minimal point of the conduction band (electrons) [37–39]. Effective mass m^* furnishes the assess the mobility of charge carriers at a given point along the $\hat{z}$ direction, according to the equation

$$\frac{1}{m*} = \frac{1}{\hbar}\frac{\partial^2 E(\vec{k} = k\hat{z})}{\partial k^2}. \quad (1)$$

Here, E is the energy of the bottom conduction band or maximum valence band, $\hbar$ is the reduced Planck's constant, and k the distance in reciprocal space.

Eq. (1) estimates the effective mass, for electron, ranging from $0.05m_0$ (at Γ along the $\Gamma \longrightarrow Y$ direction) to $1.31m_0$ (at Γ along the $Z \longrightarrow \Gamma$ direction). Regarding holes, were observed effective masses varying from $0.04m_0$ (at Γ along the $\Gamma \longrightarrow Y$ direction) to $1.18m_0$ (at B along the $B \longrightarrow D$ direction). Here, the effective mass of electron and hole is expressed in unit electron mass m_0. Besides, the previous results show that the electrons and holes transport are more favorable along the $\Gamma \longrightarrow Y$ direction, which is normal to the direction of the molecule. Our calculations reveal that electrons and holes' effective masses show an anisotropic behavior.

3.3 Optical properties

Here, we report the optical absorption of the palmitic acid crystal in its C form. Fig. 6, provides the optical absorption of the polarized incident light for some selected planes of the investigated crystal. The light absorption spectrum along the (100) and (010) directions furnishes similar behavior with a well-defined peak around the $12eV$. On the other hand, from the 5 to $10eV$ energy range, we can see a small peak along the (001) and (101) directions. The spectrum absorption curve for ($\bar{6}01$) direction, corresponding to the molecule linear direction, is similar to (100) and (010) planes. Regarding previous results, we observe evidence of weak optical anisotropy for the (001) and (101) directions in comparison to (100), (010) and ($\bar{6}01$) ones. The polycrystalline sample shows the typical overall behavior for both directions emphasizing the small peak in the 5 to $10eV$ energy range.

Fig. 7, shows the real (black line) and imaginary (red line) parts of the dielectric function taking into account distinct polarization (100), (010), (001), (101), and ($\bar{6}01$) planes for incident radiation. The dielectric function curve presents no significant difference between the real and imaginary parts for the (100), (010), and ($\bar{6}01$). The dielectric function's real part is negative only in the 5.7 to $17eV$ energy range for all cases. The imaginary part shows no negative energy in the same range as the real part. It is worth mentioning that the variation amplitudes to (001) and (101) directions exhibit no relevant variations, except to imaginary part in the 5 to $10eV$ energy range leading us to consider a weak anisotropic for these crystal directions. The polycrystalline sample shows the typical overall behavior for both directions emphasizing the small oscillations in the 5 to $10eV$ energy range.

4 Conclusions

In this work, we performed computational simulations under DFT calculations, intending to obtain the structural, electronic, and optical properties of the monoclinic palmitic acid crystal in its C form. Using $830eV$ cutoff energy, we performed LDA calculations to obtain the optimized geometry for the investigated crystal. It provided absolute deviations about 10.1%, 35.2% and 21.6% for a, b and c unit cell lattice parameters, respectively, and 56.0% for volume besides 16.5% for unit cell angle. Regarding the unit cell parameters, major deviation corresponding to c parameter around 35.2%, suggesting that such direction is flexible due to the hydrogen bond located among the adjacent planes of the palmitic acid molecule. The electronic band structure reveals indirect gap $3.713eV$ ($E \longrightarrow B$ and $E \longrightarrow \Gamma$), as a main bandgap, while the secondary bandgaps found were $4.175eV$ ($\gamma_1 \longrightarrow \Gamma$) and $4.172eV$ ($\gamma_2 \longrightarrow B$). It suggests semiconducting properties for this polymorphic form of palmitic acid. Also, the analysis of the partial density of states showed that the valence band exhibits a strong character of the p orbital for the carbon and oxygen atoms, and the s orbital for the hydrogen atom. Next, we found effective electron mass varying from $0.05m_0$ (at Γ along the $\Gamma \longrightarrow Y$ direction) to $1.31m_0$ (at Γ along the $Z \longrightarrow \Gamma$ direction). For the holes we obtained the effective mass varying from $0.04m_0$ (at Γ along the $\Gamma \longrightarrow Y$ direction) to $1.18m_0$ (at B along the $B \longrightarrow D$ direction). It reveals that the electrons and holes transport is favorable along the $\Gamma \longrightarrow Y$ direction, normal to the direction of the molecule. Also, our calculations revealed that electrons and holes effective masses are anisotropic. Optical properties behaves as an isotropic material for (100), (010), and ($\bar{6}01$) directions. The polycrystalline sample shows a typical general behavior provided by the optical absorption and dielectric function for the directions (100), (010), (001), (101) and ($\bar{6}01$). Weak anisotropy was found in the 5 to $10eV$ energy range for directions (001) and (101). In summary, our calculations suggest that the investigated palmitic acid crystal is a wide bandgap semiconductor material with potential nanotechnology applications for optoelectronic devices.

Acknowledgements We acknowledge the use of Laboratório de Física Teórica e Modelagem Computacional (LFTMC), Piripiri-PI, Brazil, and the Cluster Saturno, Fortaleza-CE, Brazil, where the calculations were performed.

Conflict of interest The authors declare that they have no conflict of interest.

Availability of data and material All data generated or analyzed during this investigation are included in this published article.

Code availability The calculations have been carried out using CASTEP Code provided by Materials Version 7.

Authors' Contribution A. Macedo-Filho and A. M. Silva prepared the first draft of this manuscript in compliance with the Ethics in Publishing Policy as described in the Guide for Authors. All authors revised and approved the final version for publication.

Funding This research was funded by the Conselho Nacional de Desenvolvimento Científico (CNPq). Grant No. 459961/2014 − 4 and 424950/2018 − 9 (A.M.F.) and 304781/2016 − 9 (E.W.S.C.).

References

1. F. F. de Sousa, G. D. Saraiva, P. T. C. Freire, J. A. Lima, P. Alcantara, F. E. A. Melo, and J. Mendes Filho, Journal of Raman Spectroscopy, 43, 146 - 152 (2012)
2. C. S. Chen, X. H. Chen, L. S. Xu, Z. Yang, Z. and W. H. Li, Carbon, 43, 1660-1666 (2005)
3. M. Bonini, E. Fratini and P. Baglioni, Materials Science and Engineering: C, 27, 1377-1381 (2007)
4. I. Simakova, O.Simakova, P. Mäki-Arvel, A. Simakov, M. Estrada and D. Yu. Murzi., Applied Catalysis A: General, 355, 100-108 (2009)
5. L. Bruni, G.Secci, S. Mancini, F. Faccenda and G. Parisi, Italian Journal of Animal Science, 19:1, 73-382 (2020)
6. K. Lipiska, A. Gumieniczek and A. A. Filip, Acta Pharm., 70, 291–301 (2020)
7. W. Luo, X. Xu, Z. Luo, J. Yao, J. Zhang, W. Xu and J. Xu, Italian Journal of Animal Science, 19:1, 8-17 (2020)
8. Y. Shang, Q. Hao, K. Jiang, M. He and Jinxin Wang, Bioorganic & Medicinal Chemistry Letters, 30, 127118 (2020)
9. F. Kaneko and H. Kubota, Current Opinion in Colloid and Interface Science, 16, 367 - 373 (2011)
10. M. Kobayashi, F. Kaneko, K. Sato, and M. Suzuki, The Journal of Physical Chemistry, 90, 6371-6378 (1986)
11. F. Kaneko, K. Tashiro and M. Kobayashi, Journal of Crystal Growth, 198/199, 1352-1359 (1999)
12. A. R. Verma and P. M. Reynolds, Proceedings of the Physical Society B, 66, 414 (1953)
13. A. R. Verma, Proceedings of the Physical Society A, 228, 34-50 (1955)
14. R. Alnoman, F. k. Al-Nazawi, H. A. Ahmed and M. Hagar, Molecules, 24, 4293 (2019)
15. M. Hagar, H. A. Ahmed and O. A. Alhaddad, 46, 2223-2234 (2019)

16. D. L. Nelson and M. M. Cox, lehninger principles of biochemistryFreeman and company, 6th, New York, 2013
17. E. Moreno, R. Cordobilla, T. Calvet, F. J. Lahoz, and A. I. Balana, Acta Crystallographica Section C, 62, 129-131 (2006)
18. E. Moreno, R. Cordobilla, T. Calvet, M. A. Cuevas-Diarte, G. Gbabode, P. Negrier, D. Mondieig, and H. A. J. Oonk, New J. Chem., 31, 947-957 (2007)
19. A. U. Chowdhury, C. M. Dettmar, S. Z. Sullivan, S. Zhang, K. T. Jacobs, D. J. Kissick, T. Maltais, H. G. Hedderich, P. A. Bishop, and G. J. Simpson, Journal of the American Chemical Society, 134, 2404-2412 (2014)
20. A. R. Verma, P. Krishna, Polymorphism and polytypism in Crystals, John Wiley and Sons Inc, New York, 1996
21. E. von Sydow, The normal fatty acids in solid state, Arkiv för kemi, Stockholm, 1956
22. K. Sato and M. Kobayashi, Crystals, Springer-Verlag, Berlin, 1991
23. F. Kaneko, M. Kobayashi, Y. Kitagawa, and Y. Matsuura, Acta Crystallographica Section C, 46, 1490-1492 (1990)
24. G. Zerbi, G. Conti, G. Minoni, S. Pison, and A. Bigotto, The Journal of Physical Chemistry, 91, 2386-2393 (1987)
25. E. Moreno-Calvo, T. Calvet, M. A. Cuevas-Diarte, and D. Aquilano, Crystal Growth & Design, 10, 4262-4271 (2010)
26. J. Gisele, Food Technology, 50, 48-83 (1996)
27. J. A. Nettleton, Omega-3 fatty acids and health, Champman and Hall, New York, 9th, 1995
28. S. M. Hirabara, R. Curi and P. Maechler, Journal of Cellular Physiology, 222, 187-194 (2010)
29. S. M. Hirabara, L. R. Silveira, L. C. Alberici, C. V, G. Leandro, R. H. Lambertucci, G. C. Polimeno, M. F. C. Boaventura, J. Procopio, A. E. Vercesi and R. Curi, Biochimica et Biophysica Acta (BBA) - Bioenergetics,1757, 56-66 (2006)
30. P. Hohenberg and W. Kohn, Phys. Rev., 136, B864-B871 (1964)
31. W. Kohn and L. J. Sham, Phys. Rev., 140, A1133-A1138 (1965)
32. B. G. Pfrommer, M. Côté, S. G. Louie and M. L. Cohen, Journal of Computational Physics, 131, 233-240 (1997)
33. M. C. Payne, M. P. Teter, D. C. Allan, T. A. Arias, and J. D. Joannopoulos, Rev. Mod. Phys., 64, 1045-1097 (1992)
34. M. D. Segall, P. J. D. Lindan, M. J. Probert, C. J. Pickard, P. J. Hasnip, , S. J. Clark and M. C. Payne, Journal of Physics: Condensed Matter, 14, 2717 (2002)
35. J. P. Perdew and A. Zunger, Phys. Rev. B, 23, 5048-5079 (1981)
36. J. P. Perdew, K. Burke, and M. Ernzerhof, Phys. Rev. Lett., 77, 3865-3868 (1996)
37. A. M. Silva, B. P. Silva, F. A. M. Sales, V. N. Freire, E. Moreira, U. L. Fulco, E. L. Albuquerque, F. F. Maia, and E. W. S. Caetano, E. W. Phys. Rev. B, 86, 195201 (2012)
38. A. M. Silva, S. N. Costa, B. P. Silva, V. N. Freire, U. L. Fulco, E. L. Albuquerque, E. W. S. Caetano, and F. F. Maia, Crystal Growth & Design, 13, 4844-4851 (2013)
39. G. Zanatta, C. Gottfried, A. M. Silva, E. W. S. Caetano, F. A. M. Sales, and V. N. Freire, The Journal of Chemical Physics, 140, 124511 (2014)

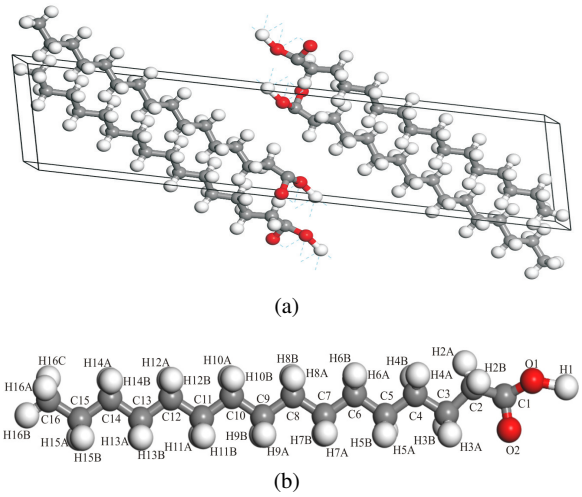

Fig. 1 1(a) Shows the palmitic-acid crystal in its C form. Carbon, oxygen, and hydrogen atoms are depicted in grey, red, and white, respectively. 1(b) Shows the isolated palmitic acid molecule in its C form.

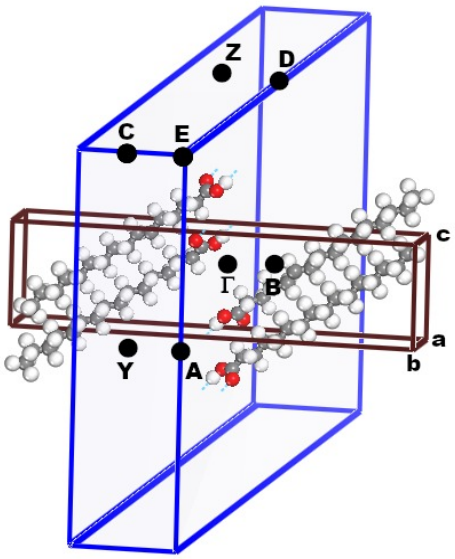

Fig. 2 First Brillouin zone of monoclinic palmitic-acid crystal in its C form showing the high-symmetry points of the reciprocal lattice. Carbon, oxygen, and hydrogen are depicted in grey, red, and white, respectively.

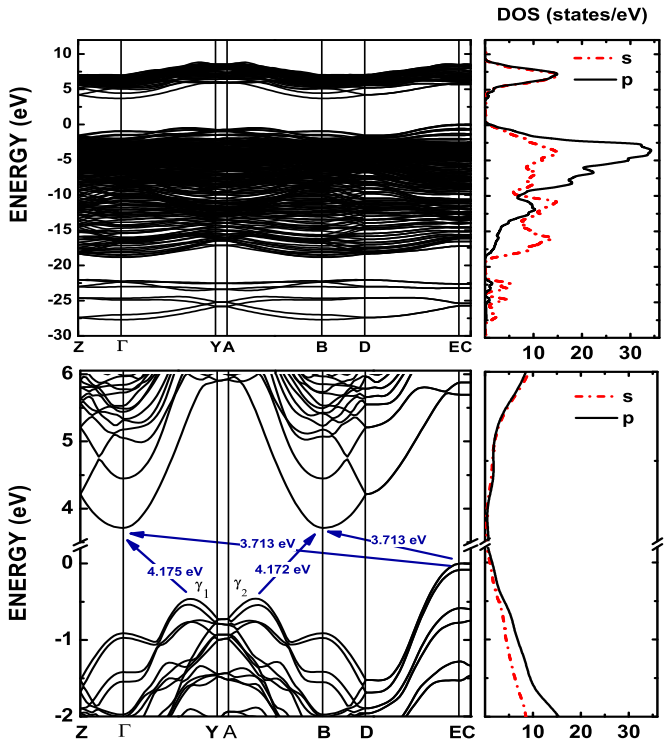

Fig. 3 (Color online) Electronic band structure calculations for the palmitic acid crystal in its C form are shown on the left side on the top and bottom Figures. The density of states (DOS) for the s (dotted) and p (solid) orbitals are shown on the right side on the top and bottom in both Figures.

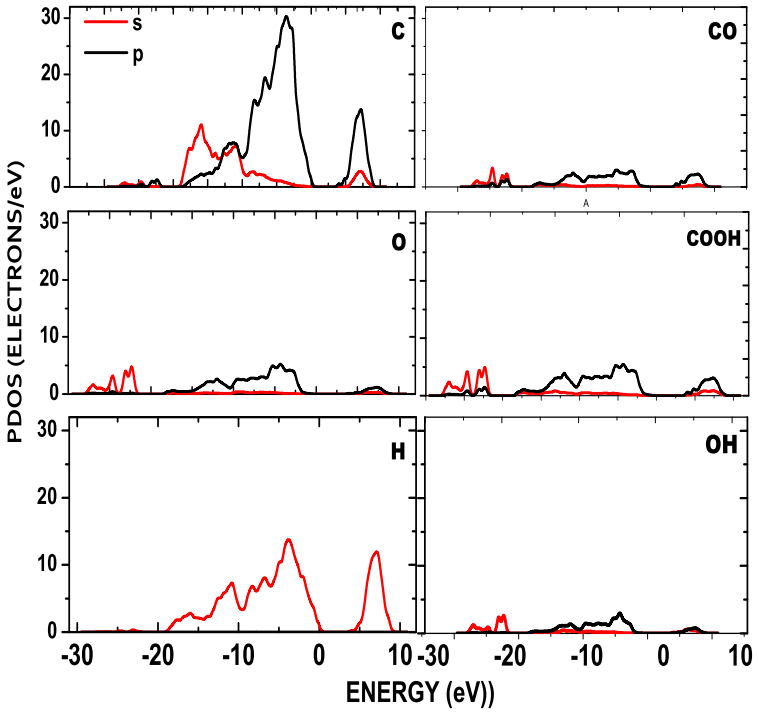

Fig. 4 (Color online) Partial electronic density of states Calculations for the palmitic acid crystal in its C form. The s (red line) and p (black line) orbitals are shown per atom (on left) and for CO (carbonyl), COOH (carboxyl), and OH (hydroxyl) functional groups (on right).

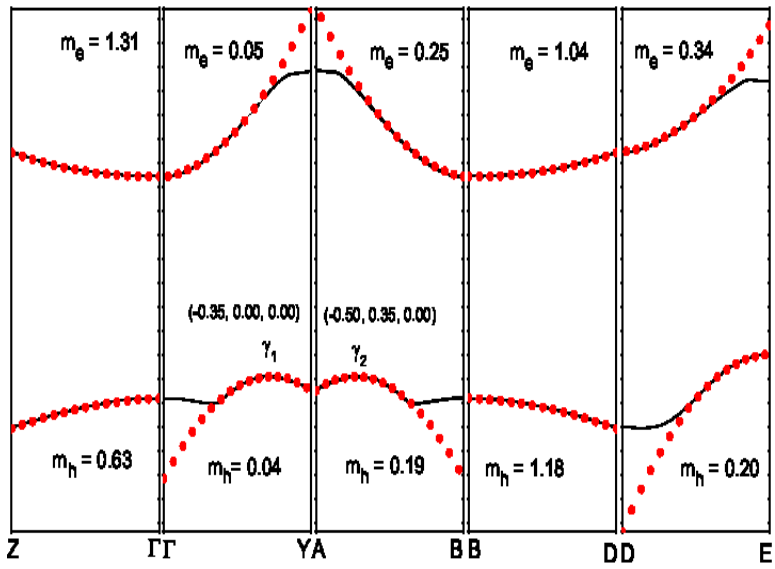

Fig. 5 (Color online) Electron and hole Effective masses (in free-electron mass unit) with performed fittings at the high- and low-symmetry points.

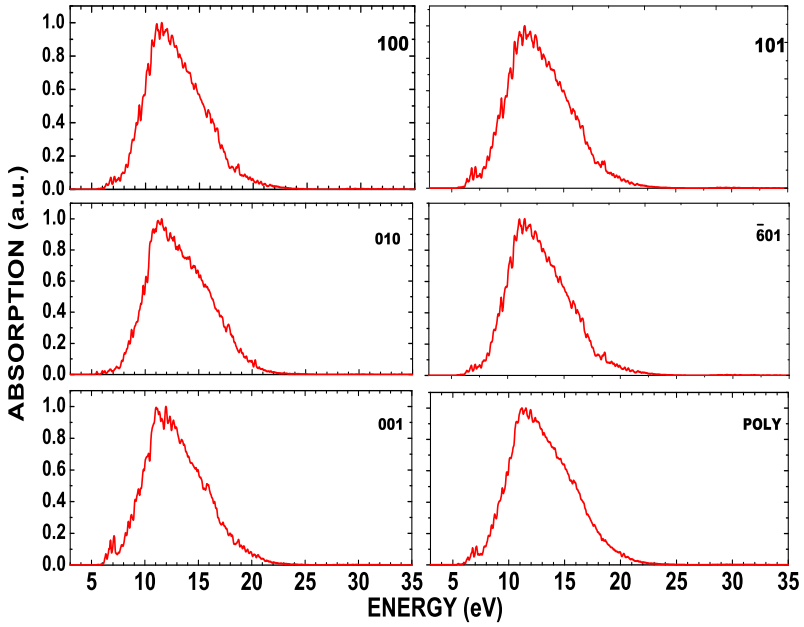

Fig. 6 (Color online) Optical absorption of the palmitic acid crystal in its C form along the (100), (010), (001), (101), and ($\bar{6}$01) planes. Optical absorption of the polycrystalline sample is shown for comparison effects.

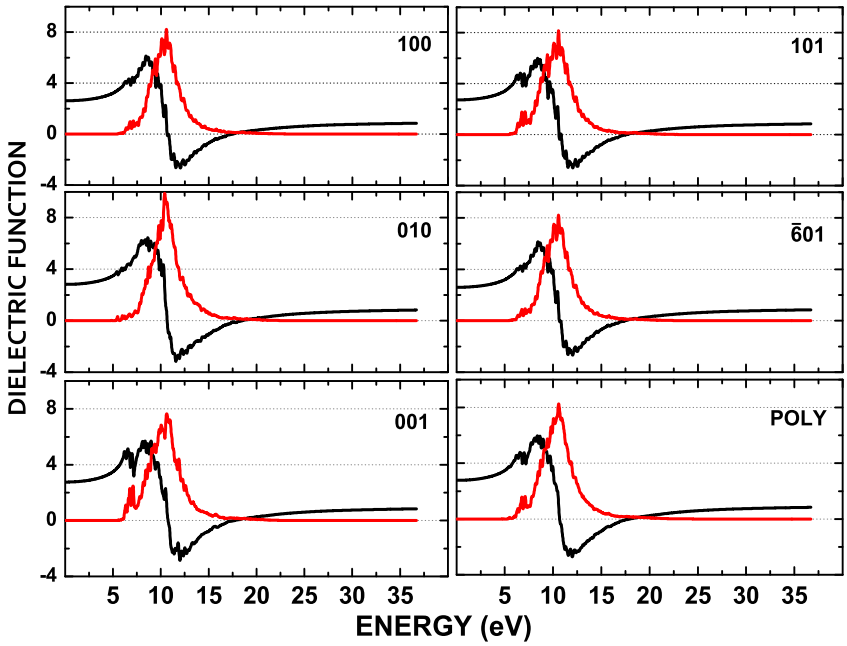

Fig. 7 (Color online) Dielectric function of the palmitic acid crystal in its C form along with the (100), (010), (001), (101), and ($\bar{6}$01) planes. Dielectric function polycrystalline sample is showed for comparison effects.

Figures

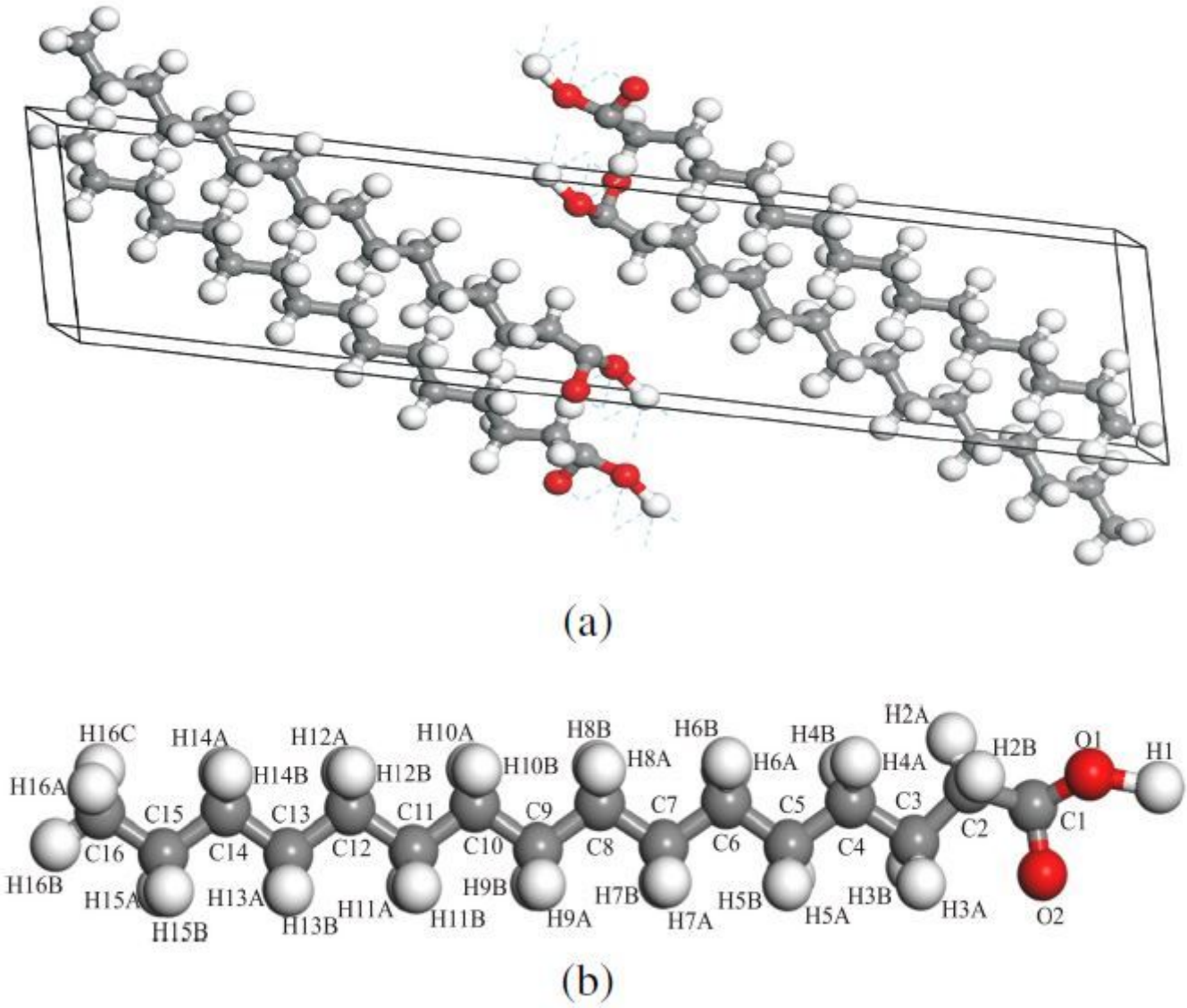

Figure 1

1(a) Shows the palmitic-acid crystal in its C form. Carbon, oxygen, and hydrogen atoms are depicted in grey, red, and white, respectively. 1(b) Shows the isolated palmitic acid molecule in its C form.

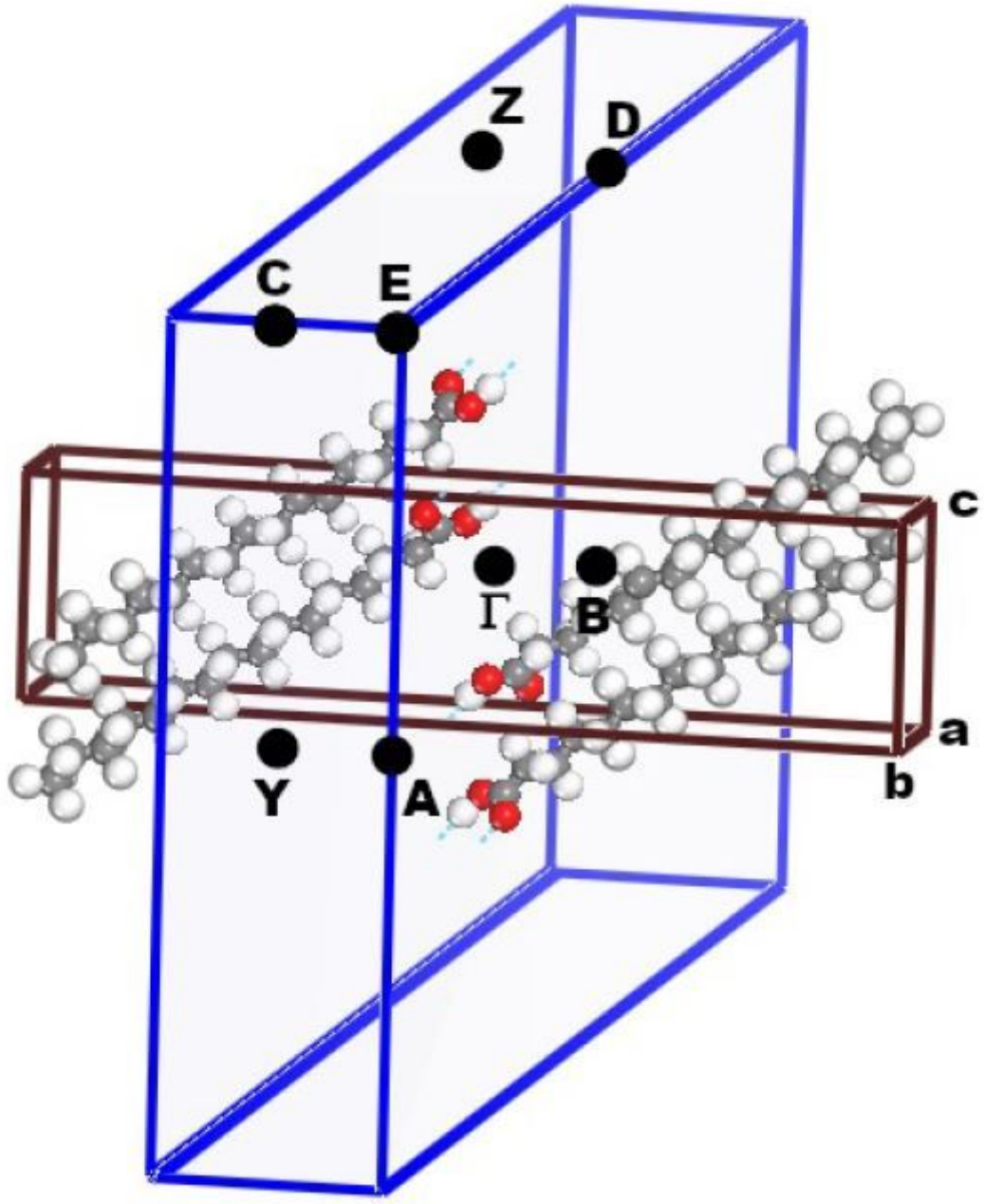

Figure 2

First Brillouin zone of monoclinic palmitic-acid crystal in its C form showing the high-symmetry points of the reciprocal lattice. Carbon, oxygen, and hydrogen are depicted in grey, red, and white, respectively.

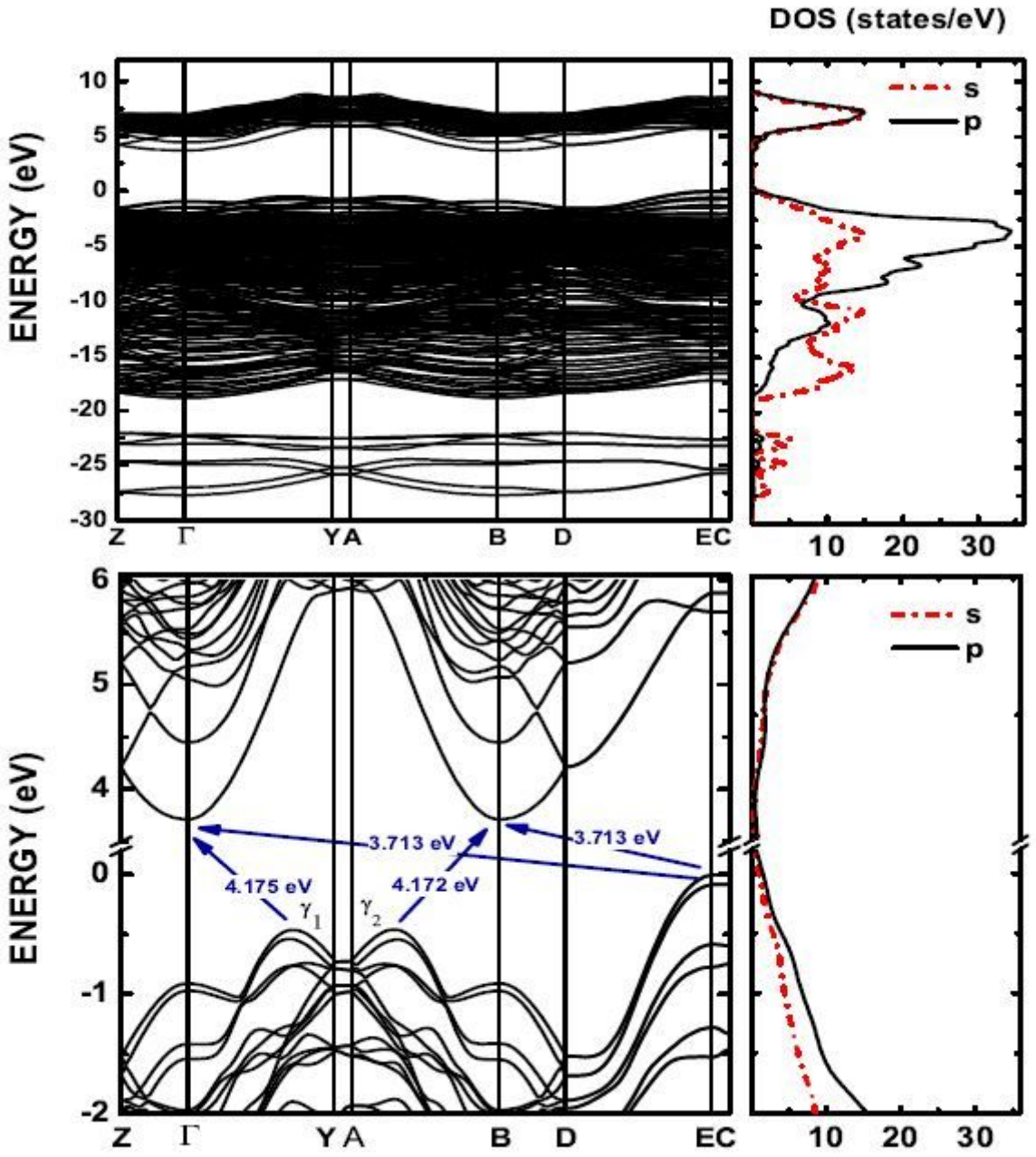

Figure 3

(Color online) Electronic band structure calculations for the palmitic acid crystal in its C form are shown on the left side on the top and bottom Figures. The density of states (DOS) for the s (dotted) and p (solid) orbitals are shown on the right side on the top and bottom in both Figures.

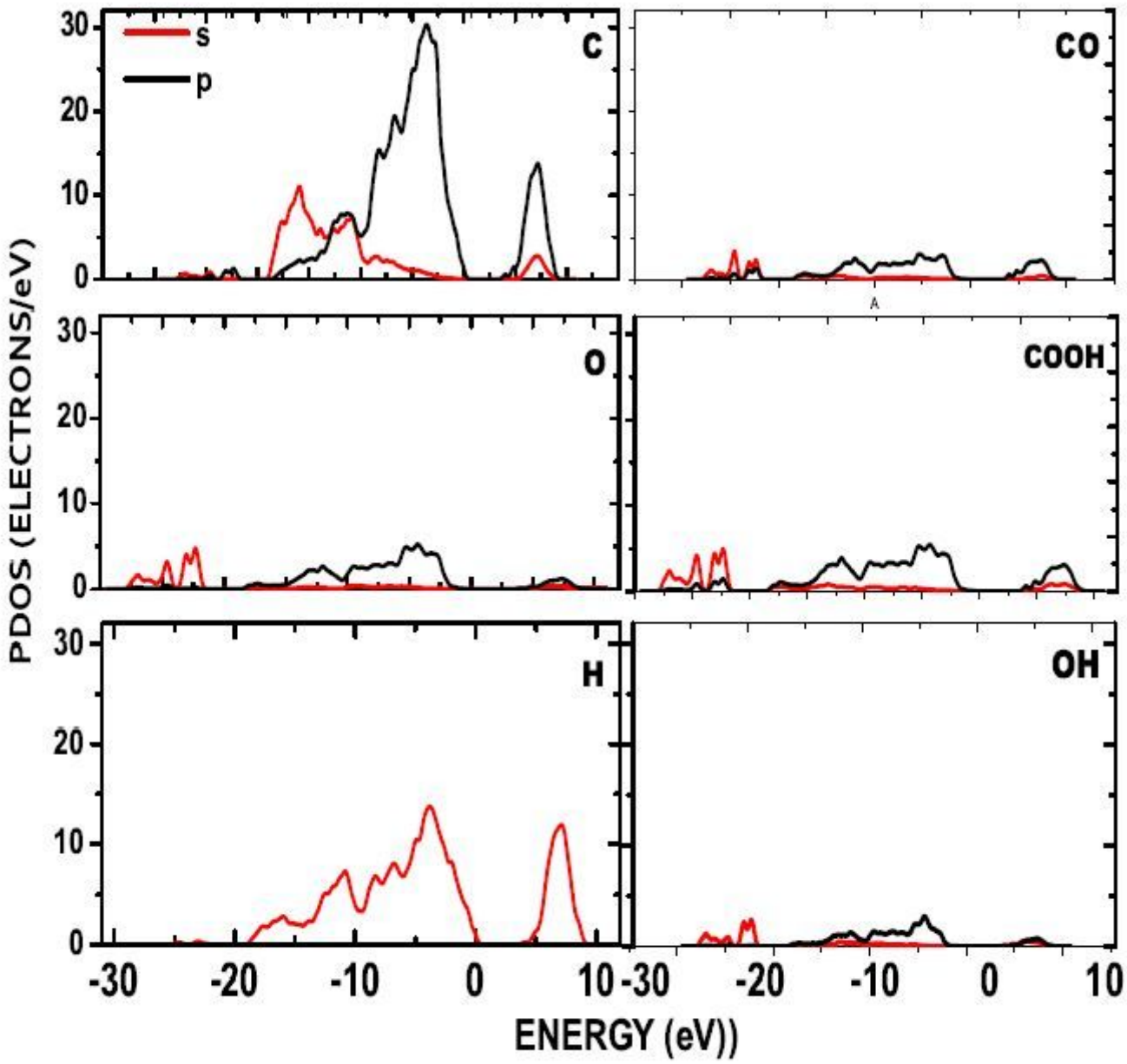

Figure 4

(Color online) Partial electronic density of states Calculations for the palmitic acid crystal in its C form. The s (red line) and p (black line) orbitals are shown per atom (on left) and for CO (carbonyl), COOH (carboxyl), and OH (hydroxyl) functional groups (on right).

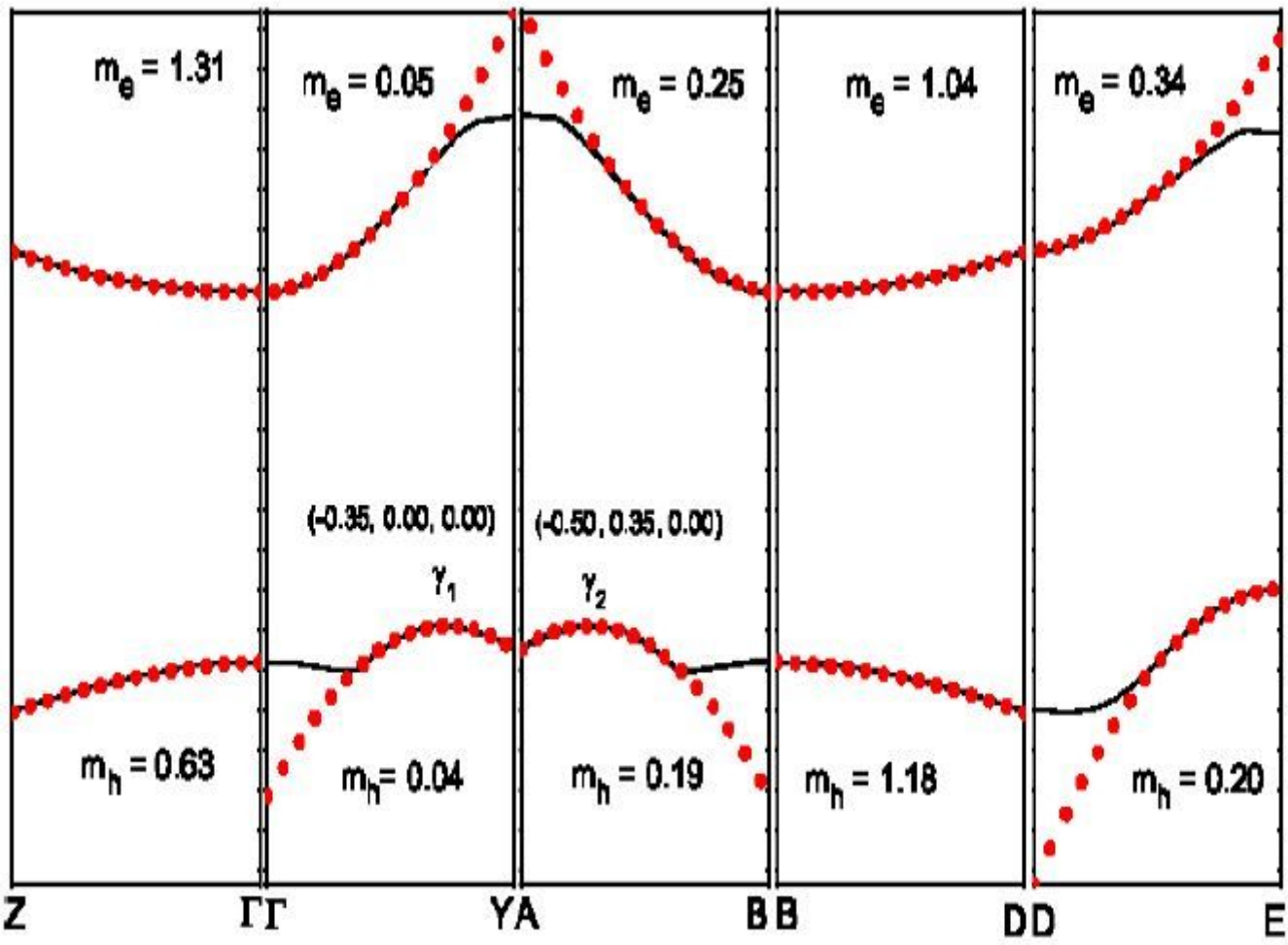

Figure 5

(Color online) Electron and hole Effective masses (in free-electron mass unit) with performed fittings at the high- and low-symmetry points.

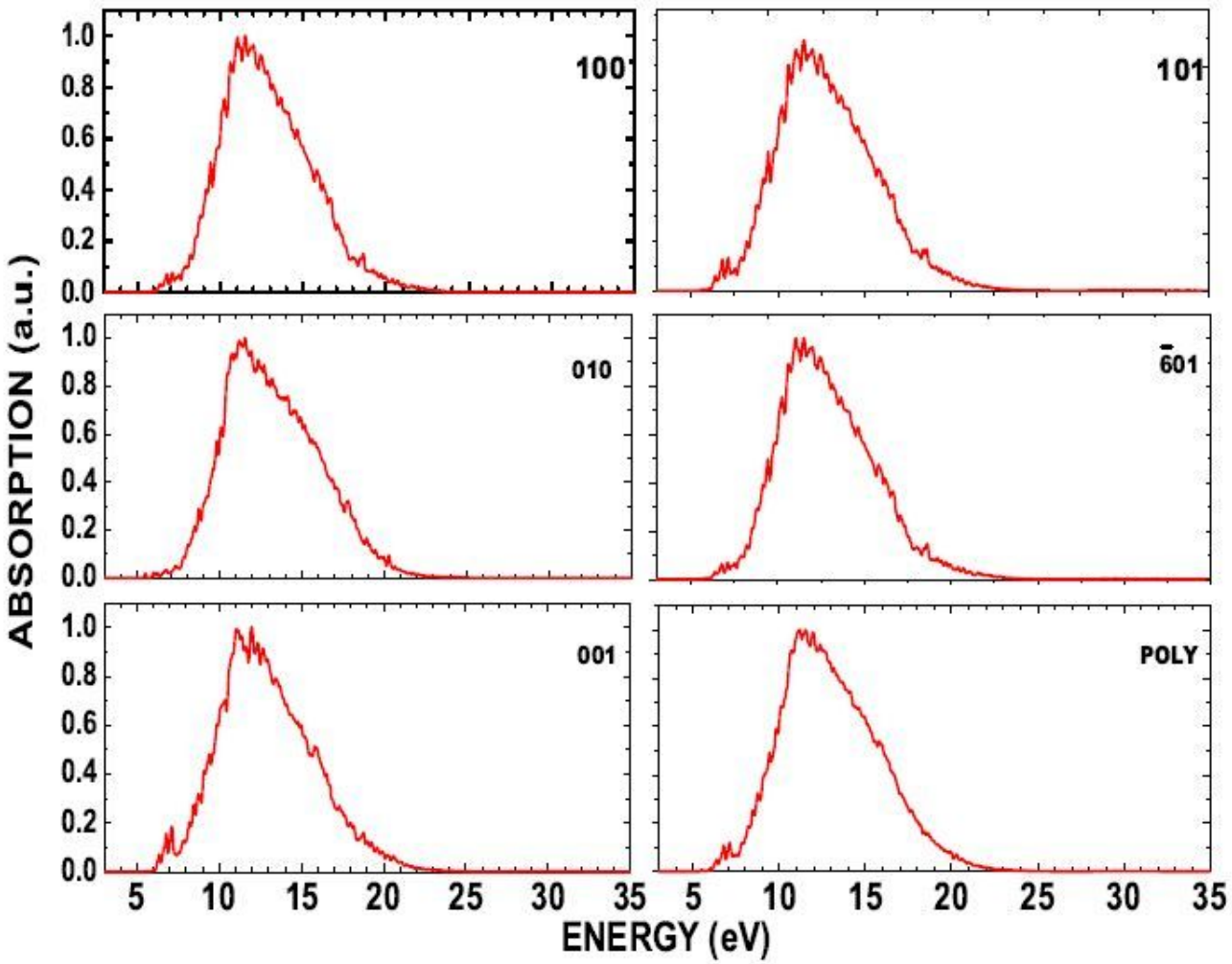

Figure 6

(Color online) Optical absorption of the palmitic acid crystal in its C form along the (100), (010), (001), (101), and ($\bar{6}01$) planes. Optical absorption of the polycrystalline sample is shown for comparison effects.

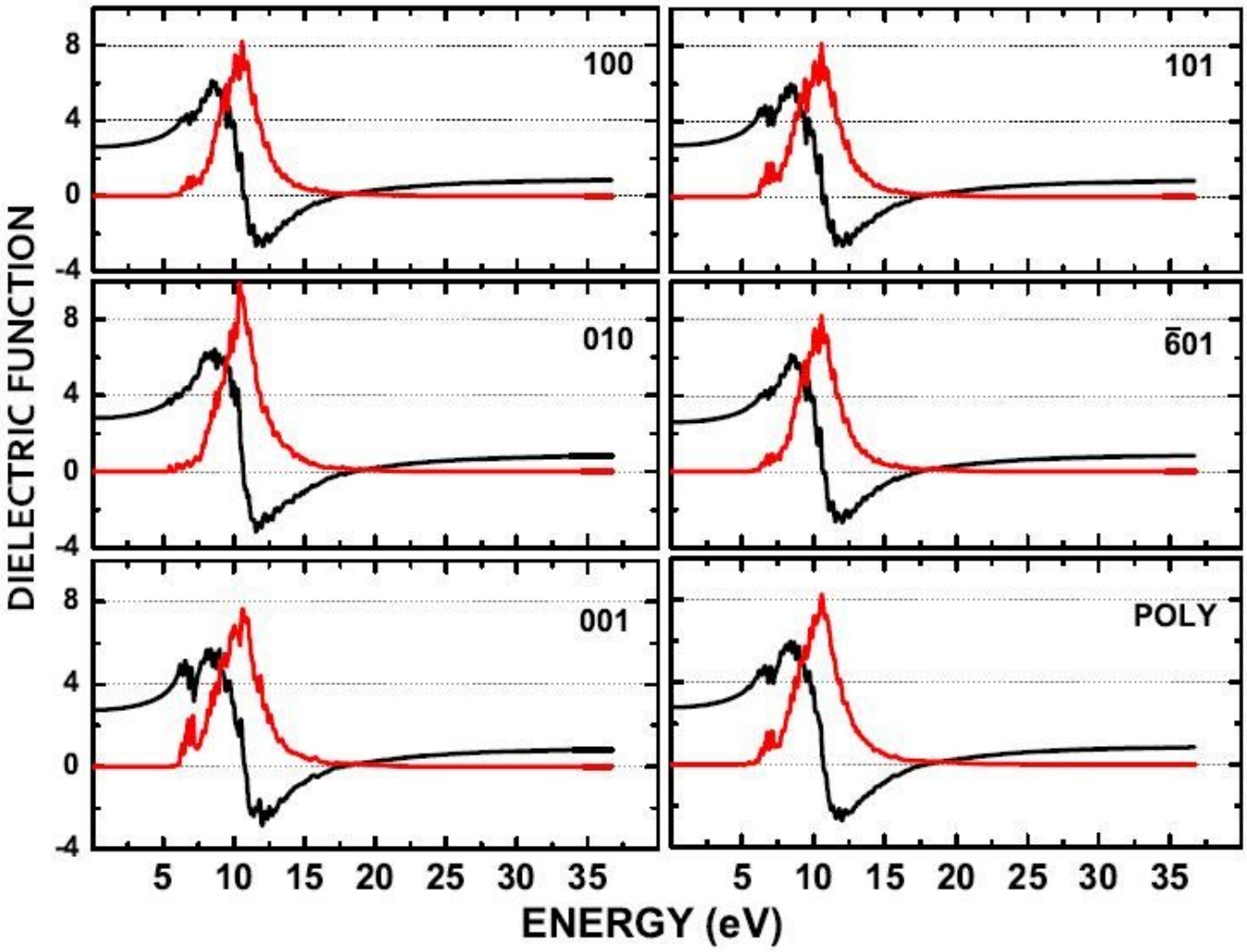

Figure 7

(Color online) Dielectric function of the palmitic acid crystal in its C form along with the (100), (010), (001), (101), and (¯601) planes. Dielectric function polycrystalline sample is showed for comparison effects.

Supplementary Files

This is a list of supplementary files associated with this preprint. Click to download.

- coverletter.pdf